

Ultrasensitive nanoparticle detection using a portable whispering gallery mode biosensor driven by a periodically poled lithium-niobate frequency doubled distributed feedback laser

Cite as: Rev. Sci. Instrum. **81**, 103110 (2010); <https://doi.org/10.1063/1.3499261>

Submitted: 19 July 2010 . Accepted: 19 September 2010 . Published Online: 27 October 2010

S. I. Shopova, R. Rajmangal, Y. Nishida, and S. Arnold



View Online



Export Citation

ARTICLES YOU MAY BE INTERESTED IN

[Protein detection by optical shift of a resonant microcavity](#)

Applied Physics Letters **80**, 4057 (2002); <https://doi.org/10.1063/1.1482797>

[Plasmonic enhancement of a whispering-gallery-mode biosensor for single nanoparticle detection](#)

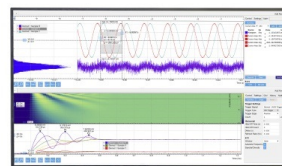
Applied Physics Letters **98**, 243104 (2011); <https://doi.org/10.1063/1.3599584>

[Nanoparticle-based protein detection by optical shift of a resonant microcavity](#)

Applied Physics Letters **99**, 073701 (2011); <https://doi.org/10.1063/1.3599706>

Challenge us.

What are your needs for periodic signal detection?



Zurich
Instruments



Ultrasensitive nanoparticle detection using a portable whispering gallery mode biosensor driven by a periodically poled lithium-niobate frequency doubled distributed feedback laser

S. I. Shopova,¹ R. Rajmangal,¹ Y. Nishida,² and S. Arnold¹

¹*MicroParticle PhotoPhysics Laboratory for BioPhotonics, Polytechnic Institute of New York University, Brooklyn, New York 11201, USA*

²*NTT Electronics Corporation, 6700-2, To, Naka-shi, Ibaraki 311-0122, Japan*

(Received 19 July 2010; accepted 19 September 2010; published online 27 October 2010)

We demonstrate a significant reduction in the limit of label-free detection of individual viral-sized nanoparticles in aqueous solution through the use of a frequency doubled telecom laser constructed from a distributed feedback-periodically poled lithium-niobate (DFB-PPLN) union. By driving a whispering gallery mode biosensor near a wavelength of 650 nm with this device we have detected real-time adsorption steps for particles 36 nm in radius with a signal to noise ratio of 8. The noise equivalent detection limit is ~ 20 ag (17 nm radius). This new lower limit is attributed to the ultralow resonance wavelength noise $[(\Delta\lambda_r)_{\text{rms}}/\lambda_r < 10^{-9}]$ associated with the use of the DFB-PPLN device. © 2010 American Institute of Physics. [doi:10.1063/1.3499261]

I. INTRODUCTION

The use of distributed feedback (DFB) telecom lasers for whispering gallery mode (WGM) resonance spectroscopy¹ substantially reduces cost in comparison with external cavity lasers (ECLs). However, a major problem with using DFB lasers for WGM biosensing² in biological fluids (e.g., blood, urine, saliva) is that readily available telecom lasers operate in the near infrared (1300–1550 nm) where water absorbs,³ causing damping of the resonator, with a corresponding loss of sensitivity.⁴ This absorption reduces the sensitivity of a WGM sensor by lowering the quality factor Q of the resonator.⁴ The same would be true of other resonant biosensors working in biological fluids, such as a photonic crystal device. Since water absorption is reduced by orders of magnitude in the visible³ most researchers and technologists have gravitated toward much more expensive, slower, and far less portable ECLs for which wavelengths are commercially available down to 633 nm. Herein we report on the use of a portable and considerably less expensive alternative. By combining a 1300 nm telecom DFB laser with a periodically poled lithium-niobate doubler (PPLN from NEL) we easily reach 650 nm. The most important advantage of using the DFB-PPLN configuration is the lack of moving parts in both the DFB laser and the PPLN frequency doubler. This allows for the design of a system that does not require vibrational isolation and can be easily transported to and used in a medical facility. In addition the lack of the ECL's mechanical tuning enables the DFB-PPLN design to be modulated much faster, which is important for following real time cavity perturbations due to bionanoparticles near the WGM surface.⁵ Beyond these advantages shorter wavelengths cause diffraction losses to be reduced, enabling the WGM structure to be scaled down, thereby increasing the wavelength shift signal.⁶ By reducing the wavelength from 1300 to 780 nm the sensitivity is increased by ~ 100 times,⁴ as demonstrated recently

by the detection of individual influenza A virus using a custom made 763 nm DFB laser system in which a DFB laser was free-space coupled to the tapered fiber.⁷ As we will demonstrate, wavelength reduction to 650 nm by using the DFB-PPLN laser along with the elimination of free-space coupling further increases the sensitivity by more than an order of magnitude. In what follows we first describe the physics of a WGM biosensor. Following this we reveal the characteristics of our DFB-PPLN laser and its use in ultrasensitive detection of individual viral size nanoparticles.

II. PHYSICS OF A WGM BIOSENSOR

The WGM biosensor is a device that confines light into a closed ring by total internal reflection (e.g., microsphere illustrated in Fig. 1). The mode is formed when light returns in phase after each circumferential passage. A WGM is easily driven into resonance by coupling light from a tunable single frequency laser by using an eroded⁸ or tapered⁹ optical fiber (current method). When the resonator is placed at a tapered fiber waist spectrally tuned light is evanescently coupled into a WGM, leading to a dip in the transmitted power spectrum [Fig. 1(a)]. The resonator may take the form of a microsphere, microdisk, or microtoroid.¹⁰ In each case total internal reflection causes light to penetrate beyond the confining dielectric structure in the form of radially decaying evanescent wave that propagates along the resonator's external perimeter. This evanescent field [illustrated by the red ribbon at the "equator" in Fig. 1(b)] provides a means for the WGM to sense its environment.

An individual DNA oligomer, protein, virus, bacteria, or arbitrary nanoparticle entering the evanescent field is polarized leading to a reactive shift of the resonator's frequency.⁶ This interaction actually results in two closely spaced dips since the perturbing nanoparticle splits the clockwise/counterclockwise degeneracy.¹¹ In our experiments such fine

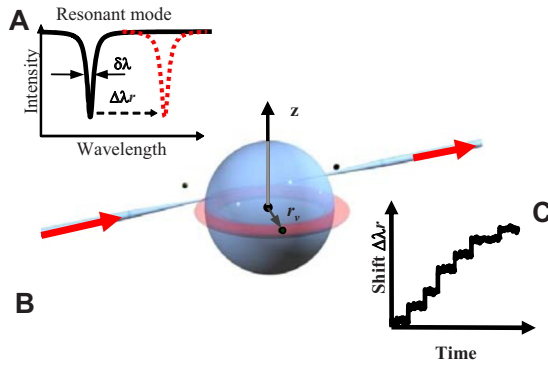


FIG. 1. (Color online) (a) A resonance spectrum before (black line) and after adsorption (dashed red line); (b) a microsphere stimulated into a WGM by light evanescently coupled from a tapered fiber; (c) binding curve illustrating possible steps in $\Delta\lambda_r$ with time.

structure is not seen since the measured single particle shift $(\Delta\lambda_r)_{np}$ is much smaller than the linewidth $\delta\lambda_r$ of the dip. This is the circumstance in the large majority of sensing experiments using WGMs. In this limit the theoretical description is simple. The fractional single nanoparticle shift $(\Delta\lambda_r)_{np}/\lambda_r$ is equal to the polarization energy divided by the energy in the cavity mode (reactive sensing principle). In electrical terms⁶

$$\frac{(\Delta\lambda_r)_{np}}{\lambda_r} \approx \frac{\alpha_{ex} |\mathbf{E}_0(\mathbf{r}_v)|^2}{2 \int \varepsilon_s |\mathbf{E}_0(\mathbf{r})|^2 dV} \quad (1)$$

where α_{ex} is the excess polarizability of the nanoparticle, ε_s is the permittivity of the cavity, and $\mathbf{E}_0(\mathbf{r}_v)$ and $\mathbf{E}_0(\mathbf{r})$ are modal field amplitudes at the position of the nanoparticle \mathbf{r}_v and throughout the mode, respectively. As a particle binds, a step is seen in the wavelength shift in proportion to the particle's polarizability, which in turn is proportional to the particle's volume and mass. These steps become uniform if the binding sites share a common intensity, as they do for points on the equator [as illustrated in Fig. 1(c)]. Light forces promote binding at the equator as demonstrated in Ref. 5. Although Eq. (1) provides theory for the shift that can be expected, the ever-present noise that keeps us from detecting an arbitrarily small polarizability is determined by a host of factors. Of these, for a portable device, we have found vibrational isolation to be the most difficult to overcome. Before discussing our sensing results we will describe the construction of the laser and measurement system.

III. DFB-PPLN LIGHT SOURCE AND ITS INTEGRATION WITH THE WGM BIOSENSOR

Figure 2 shows the schematic of the DFB-PPLN light source and its integration with the WGM sensor.

The source for frequency doubling is a pig-tailed 1304 nm DFB telecom laser (NLK1B5GAAA). The pig-tail is a polarization maintaining (PANDA 1300 nm) fiber which is connected to the input fiber (PANDA 1300 nm) of the wavelength conversion module (WH-0650-000-F-B-C) with a SC/PC connector. The wavelength of the DFB laser was principally controlled by its current that was scanned with a dc offset saw tooth waveform. The temperature of the DFB was held constant to better than 0.01 °C. The wavelength conversion module consists of a periodically poled (11.8 μm period) ZnO-doped LiNbO₃ (PPLN) waveguide (8 \times 8 μm core, 34 mm long) that allows for doubling the frequency of the laser source. The ZnO doping makes the PPLN highly resistant to photorefractive damage. The quipphase matched (QPM) condition¹² for efficient second harmonic generation is achieved by adjusting the PPLN temperature. For this purpose we built a small temperature control unit (WTC3243-Wavelength Electronics' chip, Wavelength Electronics, Bozeman, MT), that stabilizes the temperature to less than 0.01 °C. The PPLN unit was input and output pigtailed for convenient light delivery to a polarization controller followed by the microsphere sensing unit. PPLN chip output was outcoupled by a single mode (for 750 nm) fiber terminated by a FC/APC connector. To promote coupling to the microsphere the fiber is tapered to $\sim 2 \mu\text{m}$ at the point of contact with the resonator. Both the tapered fiber and resonator were enclosed in a microfluidic cell.⁴ The previously mentioned polarization controller allows for selecting the WGM polarization [i.e., transverse electric (TE) or transverse magnetic (TM)]. The sensor is actually a microspheroid that is formed by melting the tapered tip of a silica fiber with the focused beam of a CO₂ laser. This procedure allows for good control of the resonator size. Beyond the microsphere the fiber is led to a universal silicon detector (Newport 818-IS-1) for transducing the transmitted power. A computer running LABVIEW records this transmitted signal after receiving a trigger signal from the function generator.

IV. DFB-PPLN LASER CHARACTERISTICS

With the PPLN doubler held at an operating temperature $T_{op} = 26.4 \text{ }^\circ\text{C}$, the QPM condition occurred for the DFB laser tuned to 1303.485 nm. Figure 3 shows the output frequency-

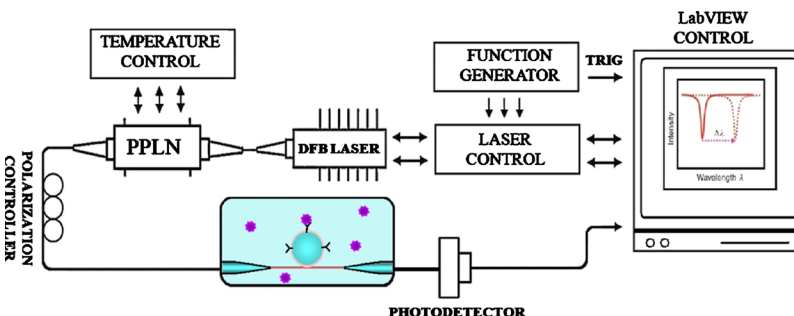


FIG. 2. (Color online) Schematics of DFB-PPLN-WGM sensing system.

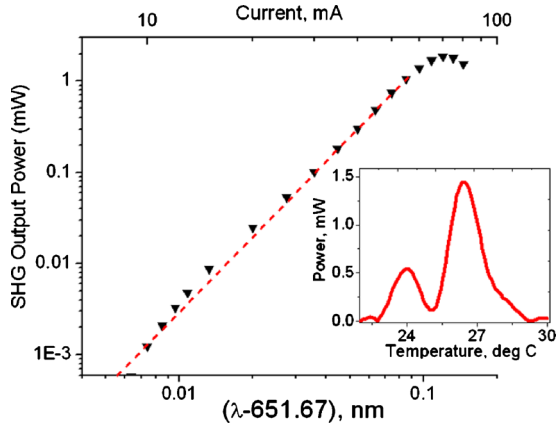


FIG. 3. (Color online) NEL-PPLN output power as a function of frequency doubled wavelength (lower) and DFB drive current (upper). The maximum output power at 651.742 ± 0.002 nm was 1.86 mW for a DFB input power of 17.8 mW. The inset shows the output as a function of PPLN operating temperature for a slightly smaller input power.

doubled power as the DFB laser is tuned below the QPM wavelength. Continuous tuning in the red is apparent. The second harmonic generated power as a function of the PPLN temperature is also shown as an inset within the figure.

The maximum output power at 651.742 nm was 1.86 mW for a DFB input power of 17.8 mW. The efficiency of the PPLN device is often represented as the percent of power conversion per milliwatt of input power. On this basis the doubler has an efficiency at its maximum of 0.587%/mW. In practice the laser is operated near its QPM temperature in order to minimize variations in the output power with DFB drive current.

V. SENSING RESULTS

The value of the DFB-PPLN laser for WGM sensing is best revealed from single nanoparticle binding experiments in aqueous solution. The experiment described in what follows is typical of our results and represents the smallest nanoparticle detected and analyzed by reactive WGM sensing in aqueous solution.

Figure 4 shows a particular experiment in which nanoparticles (Polysciences polystyrene hydrosol with mean particle radius $\langle a_v \rangle = 40$ nm) surround a microsphere of radius $R = 35$ μm at a concentration of ~ 10 fM. Clear adsorption and desorption events are seen. Such a particle size would have been near noise levels in our earlier single virus particle measurements.⁷ The ability to see these events so clearly is due to (1) the ultralow noise associated with the intrinsic vibrational isolation afforded by the elimination of free-space coupling to the tapered fiber, and (2) the reduction in wavelength provided by the DFB-PPLN union. The reduced noise produces a rather profound effect. Although the same resonance tracking algorithm, current driver, and detection bandwidth were used in Ref. 7, the fractional preinjection root mean square noise $(\Delta\lambda_r)_{\text{rms}}/\lambda_r$ in that experiment (3×10^{-9}) was three times larger than we measured in our current experiment; $(\Delta\lambda_r)_{\text{rms}}/\lambda_r$ is currently 1×10^{-9} . In what follows we will interpret our data and estimate a noise equivalent limit of detection (LOD).

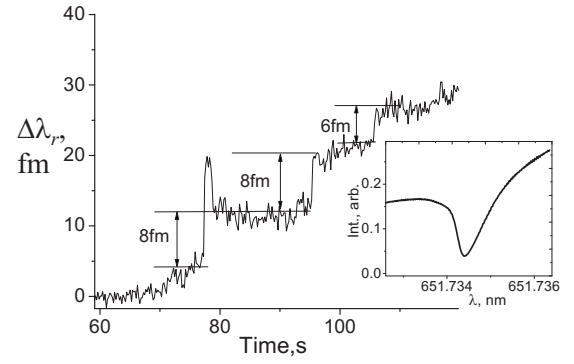


FIG. 4. Shift of resonance wavelength of a microsphere resonator ($R = 35$ μm) in time after polystyrene particles from a hydrosol with a concentration $\sim 10^{-14}$ M and mean radius $\langle a_v \rangle = 40$ nm were injected into the surrounding microfluidic cell. The inset shows the recorded resonance line ($Q \approx 10^6$). Points were taken 1/5 s apart while maintaining a bandwidth of $\sim 10^3$ Hz. The power coupled into the sphere from a tapered fiber was 52 μW .

VI. INTERPRETATION OF SENSING RESULTS

For the equatorial mode depicted in Fig. 1, the largest wavelength shift is expected for nanoparticles binding on the equator where the mode has its largest intensity; where $|\mathbf{E}_0(\mathbf{r}_v)|^2$ in Eq. (1) is largest. This is also the region where nanoparticle binding is promoted by light forces, since the attractive gradient force peaks at the equator.⁵ An expression for this optimal shift has been derived from Eq. (1) for this case⁷

$$\begin{aligned} \left[\frac{(\Delta\lambda_r)_{sp}}{\lambda_r} \right]_{\text{max}} &\approx \frac{\alpha_{\text{ex}} |\mathbf{E}_0(r=r_v, \theta=\pi/2)|^2}{2f\epsilon_s |\mathbf{E}_0(r)|^2 dV} \\ &\equiv D \frac{a_v^3}{R^{5/2} \lambda_r^{1/2}} e^{-a_v/L}, \end{aligned} \quad (2)$$

where D is a dielectric factor (which for polystyrene in water is 2.25) and L is the characteristic length of the evanescent intensity.¹³ The a_v (Ref. 3) factor reflects the fact that the shift is proportional to the polarizability, which is proportional to the particle volume, and the exponential $e^{-a_v/L}$ accounts for the evanescent intensity fall-off from the surface to the center of the nanoparticle. The inverse dependence on $R^{5/2}$ indicates, as verified recently,⁷ that the shift is approximately inversely proportional to the WGM mode volume. Based on the reactive mechanism the radius of the nanoparticle may be estimated from our experimental data by inverting Eq. (2); solving for a_v .

In the limit in which the particle radius a_v is small in comparison with the evanescent intensity length L , the solution to Eq. (2) is

$$a_0 = \frac{R^{5/6} \lambda_r^{1/6}}{D^{1/3}} \left[\frac{(\Delta\lambda_r)_{\text{np}}}{\lambda_r} \right]_{\text{max}}^{1/3}. \quad (3)$$

However in general $a_v = -3LW[-a_0/(3L)]$, where W is the Lambert product log function. Fortunately the series expansion for this function is well known. In terms of the argument $\xi = a_0/(3L)$ which for our experiments is ~ 0.1 , the nanoparticle radius to third order in ξ is¹⁴

$$a_v = a_0[1 + \xi + (3/2)\xi^2 + (3/8)(\xi^3) + O(\xi^4)\dots]. \quad (4)$$

For the experiment shown in Fig. 4 using a silica microsphere resonator ($R=35 \pm 0.5 \mu\text{m}$), the maximum steps in adsorption and desorption at a wavelength of $\lambda_r=651.7 \text{ nm}$ is $(\Delta\lambda_r)_{\text{np}}=8 \pm 1 \text{ fm}$. The dielectric nanoparticle radius is computed from Eqs. (3) and (4) to be $a_v=36 \pm 2 \text{ nm}$, using dielectric factor $D=2.26$ and the characteristic length $L=89.8 \text{ nm}$.¹³ Our result is in excellent agreement with the hydrosol mean size of $40 \pm 5 \text{ nm}$. This represents the smallest individual particle detected and sized in aqueous solution, but it is by no means the LOD.

VII. LOD FOR THE DFB-PPLN DRIVEN WGM BIOSENSOR

The current LOD is based on the fluctuations in the resonance wavelength before any adsorption takes place. With the setup in Fig. 2 this relative fluctuation is $(\Delta\lambda_r)_{\text{rms}}/\lambda_r \approx 10^{-9}$. Substituting this for the fractional shift in a_0 , [Eq. (3)] we arrive at the size LOD, where $a_{0,\text{rms}} = [(R^{5/6}\lambda_r^{1/6})/D^{1/3}][(\Delta\lambda_r)_{\text{rms}}/\lambda_r]^{1/3}$ and $\xi = a_{0,\text{rms}}/(3L)$. Our estimate for a_{LOD} is $17 \pm 2 \text{ nm}$, which is smaller than most human virus.

VIII. CONCLUSIONS

We have demonstrated an application of a new laser source, based on a telecom DFB laser and PPLN doubler, for driving WGMs resonators. The extremely low noise of this source allowed for achieving the lowest reported detection limit for single particle detection in aqueous solutions. The LOD was represented in a simple series expansion which is applicable in evaluation of LOD for any WGM geometry.

The work is also a significant step in design of portable and inexpensive biosensing devices applicable in clinical settings.

ACKNOWLEDGMENTS

The authors want to thank NEL for the loan of PPLN device and the National Science Foundation for supporting this work (Grant No. CBET 0933531).

- ¹G. Griffel, S. Arnold, D. Taskent, A. Serpengüzel, J. Connolly, and N. Morris, *Opt. Lett.* **21**, 695 (1996).
- ²F. Vollmer and S. Arnold, *Nat. Methods* **5**, 591 (2008).
- ³G. M. Hale and M. R. Querry, *Appl. Opt.* **12**, 555 (1973).
- ⁴S. Arnold, R. Ramjit, D. Keng, V. Kolchenko, and I. Teraoka, *Faraday Discuss.* **137**, 65 (2008).
- ⁵S. Arnold, D. Keng, S. I. Shopova, S. Holler, W. Zurawsky, and F. Vollmer, *Opt. Express* **17**, 6230 (2009).
- ⁶S. Arnold, M. Khoshshima, I. Teraoka, S. Holler, and F. Vollmer, *Opt. Lett.* **28**, 272 (2003).
- ⁷F. Vollmer, S. Arnold, and D. Keng, *Proc. Natl. Acad. Sci. U.S.A.* **105**, 20701 (2008).
- ⁸A. Serpengüzel, S. Arnold, G. Griffel, and J. A. Lock, *J. Opt. Soc. Am. B* **14**, 790 (1997).
- ⁹J. C. Knight, G. Chung, F. Jacques, and T. A. Birks, *Opt. Lett.* **22**, 1129 (1997).
- ¹⁰X. Fan, I. M. White, S. I. Shopova, H. Zhu, J. D. Suter, and Y. Sun, *Anal. Chim. Acta* **620**, 8 (2008).
- ¹¹J. Zhu Sahin, S. K. Ozdemir, Y. F. Xiao, L. Li, L. He, D. R. Chen, and L. Yang, *Nat. Photonics* **4**, 46 (2010).
- ¹²M. M. Fejer, G. A. Magel, D. H. Jundt, and R. L. Byer, *IEEE J. Quantum Electron.* **28**, 2631 (1992).
- ¹³ $L \approx (\lambda/4\pi)(n_s^2 - n_m^2)^{-1/2}$, $D = 2n_m^2(2n_s)^{1/2}(n_{np}^2 - n_m^2)/(n_s^2 - n_m^2)(n_{np}^2 + 2n_m^2)$, where n_s , n_m , and n_{np} are the refractive indices of the microsphere (1.45), aqueous medium (1.33), and polystyrene (1.59); for polystyrene nanoparticles $D=2.26$.
- ¹⁴R. M. Corless, D. J. Jeffrey, and D. E. Knuth, *Proceedings of the 1997 International Symposium on Symbolic and Algebraic Computation*, Maui, HI (ACM, New York, 1997), pp. 197–204.